3

Velocity Distributions in Potassium Molecular Beams*

P. M. MARCUS and J. H. McFEE

Carnegie Institute of Technology
Pittsburgh, Pennsylvania

I. Introduction

This paper describes velocity distribution measurements made on potassium molecular beams with a fixed-frequency, variable phase velocity selector. The measurements are believed to be of high accuracy, and were taken over a wide range of oven pressures (0.84×10^{-3} mm Hg to 0.58 mm Hg).

The work described here is a continuation of work by A. Bennett and I. Estermann. The molecular beam apparatus was designed and constructed by Bennett[1] who also used the equipment to measure the velocity distribution in potassium beams. Comparison of his results with the Maxwell-Boltzmann distribution showed the marked effects of oven-slit geometry on the velocity distributions, and indicated a substantial deficiency of low-velocity molecules at moderately high oven pressures.[1] In all these measurements there was an uncertainty in the transit time of molecules passing through the selector of about 3% of the most probable transit time. If the measured and calculated most probable transit-times agreed to within this uncertainty, a factor was applied which made the position of the peaks coincide. Since Bennett's work, a number of refinements (which are described below) have been made which permit more accurate velocity measurements. In particular, a more accurate method of transit-time measurement has been devised, and no adjustment is now made in the position of the maximum of the measured velocity distribution when comparing it to the theoretical distribution. The uncertainty in the transit time is now less than 1% of the most probable transit time. Comparison of the present measurements with theoretical curves derived from the

Maxwell distribution indicates a considerable deficiency of low-velocity molecules at the highest oven pressures. At the lowest oven pressures there is good agreement between the measured and theoretical curves.

Measurements of the velocity distribution in a potassium beam after reflection from a solid surface are now being attempted. Comparison of these with the direct-beam measurements should yield detailed information about the energy exchange between the beam and the surface.

II. Description of Apparatus

(a) General

Figure 1 is a plan view of the beam apparatus. An expanded scale is used for the slits to show their relative size. The "collimating" slit

TOP VIEW OF BEAM APPARATUS

OVEN SLIT WIDTH   0·06 MM
COLLIMATING SLIT WIDTH   0·40 MM
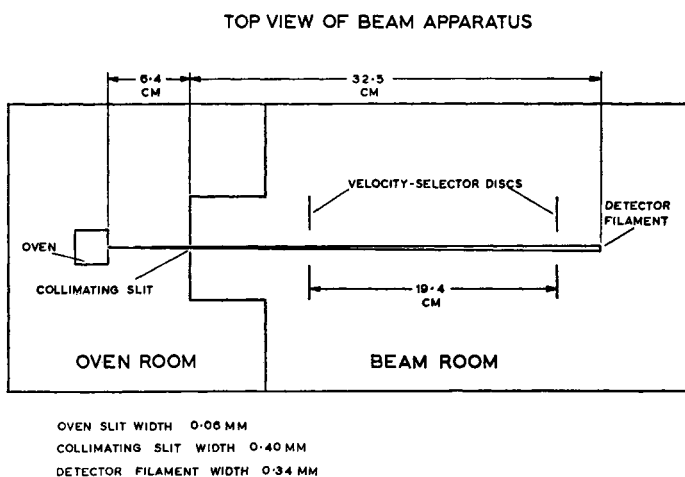DETECTOR FILAMENT WIDTH   0·34 MM

Fig. 1. Top view of beam apparatus showing dimensions. Expanded scale was used for slits and detector filament.

is narrow enough to provide sufficient isolation of the beam room from the oven room, but it does not define the beam. The beam is defined by the oven slit and the detector filament so that the effective path of the beam can be changed by moving the detector filament. The oven, velocity selector and detector are mounted on an optical bench and aligned optically, then inserted in a cylindrical vacuum chamber. The circular plate on the left divides the chamber into the separate oven, room and beam room.

(b) *Oven*

The oven shown in Fig. 2 is made entirely from copper to minimize thermal gradients. The potassium, sealed in a glass capsule, is placed in a hole in the plug. The front end of the capsule is broken off by pressure when the plug is tightened. The plug is chrome-plated to prevent jamming of copper threads. Clogging of the slits due to creep of potassium is minimized by holding the capsule in a vertical position.
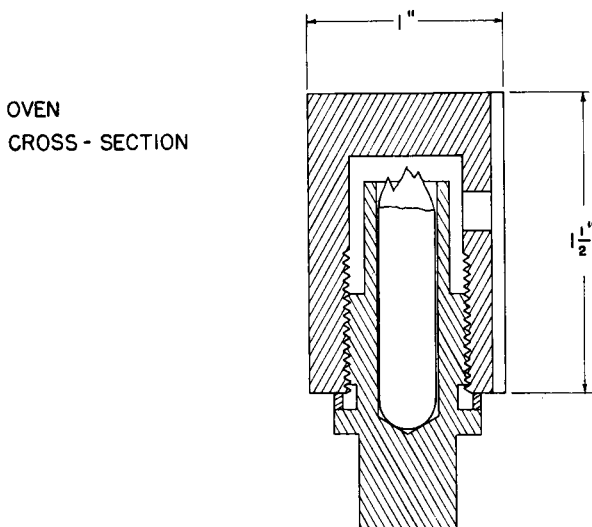

OVEN

CROSS - SECTION

Fig. 2. Oven cross-section (side view) showing threaded plug holding capsule of potassium.

(c) *Oven Slit*

In all the measurements described in this paper, thin foil (0.001 in. stainless steel) slit edges were used. The oven slit construction is practically identical with the "ideal" slit used by Miller and Kusch.[2]

(d) *Detector*

A surface-ionization detector was used, consisting of a strip 2 cm long × 0.3 mm wide × 0.002 in. thick, rolled out from suitable Pt, Mo, or W wire. Pt and Mo were found to be most satisfactory for measuring weak beams since the positive-ion background current emitted by these metals is very small in comparison to W. (Various W specimens were tried, including some "undoped" specimens by courtesy of Mr. J. S. Petro of the General Electric Company Lamp Wire and Phosphors Dept.)

A direct test for possible velocity sensitivity of the detecting filament was made by taking two successive velocity spectra differing only by substitution of a Pt for a W filament (by internal exchange of the filaments). The spectra showed identical relative intensity distributions, although the Pt detection efficiency was only about 80% of the W detection efficiency.

An Applied Physics Corp. Mod. 31 vibrating-reed electrometer was used to measure the ion current produced by the detector.

(e) Velocity-selector

The velocity selector consists of two identical slotted discs (Fig. 3). Each disc is turned by an 8000 rpm synchronous motor. A phase-shifter* varies the phase of the voltage fed to one motor relative to the
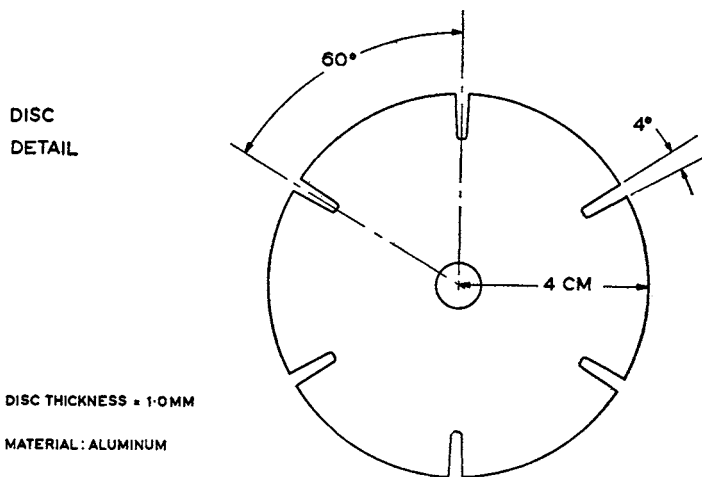

Fig. 3. Detail of selector disc.

other. As is described below, a light beam is used to determine when the velocity selector is set for zero transit-time. This beam is produced by a small light source near one disc. It then passes through the velocity selector underneath the motors, and is detected by a photo-cell near the other disc. The motors use miniature precision ball bearings which are lubricated when installed with a small drop of diffusion pump oil. A pressure of $\leqslant 5 \times 10^{-7}$ mm Hg can be maintained indefinitely in the beam room with the motors running.

* A differential generator (i.e. a type of transformer in which one winding can be rotated with respect to the other) is used as a phase-shifter.

III. Action of the Velocity-Selector

As explained in Appendix I, if the setting of the phase-shifter is such that the delay time of the second disc relative to the first is τ, and the slit open time is β, then the number of beam particles passing through the selector (per cm² of beam cross-section) each time a pair of slits—one slit in one disc, one slit in the other disc—cuts the beam (call this one pass) will be given by

$$h(\tau, \beta) = \int_0^\infty S(\tau, T, \beta) I(T) dT. \tag{1}$$

T is the transit time (between discs of separation l), $I(T)dT$ is the incident intensity in the range dT (molecules/cm² sec) and $S(\tau, T, \beta)$ is the "shutter function" (secs) describing the transmission of the velocity selector for a given phase setting (it is the effective open time in a single pass for molecules of transit time T).

If the effusion from the oven is ideal, $I(T)$ will simply be the "Maxwell beam intensity function" (ref. 4, p. 20), in the transit-time variable. It is convenient to use dimensionless variables obtained by dividing by T_0, the transit-time of the most probable velocity in the oven. Defining the reduced transit-time

$$\bar{T} = \frac{T}{T_0} \text{ where } T_0 = l \Big/ \sqrt{\frac{2R T_K}{M}}; \ T_K = \text{absolute temperature} \tag{2}$$

we have

$$I(T) dT = \frac{2I_0}{\bar{T}^5} e^{-(1/\bar{T})^2}.d\bar{T}, \tag{3}$$

which has a form independent of temperature. I_0 is the total beam intensity (molecules/cm² sec). $I(T)$ is plotted as the solid curve in Fig. 4.

The shutter function $S(\tau, T, \beta)$ is an isosceles triangle as a function of T, base 2β, peak β (at $T = \tau$), if beam width and disc thickness are negligible. The reduced shutter function S/T_0 is shown in Fig. 4, (for typical values of $\beta = 0.850 \times 10^{-4}$ sec and $T_0 = 4.557 \times 10^{-4}$ sec). Since T_0 depends on temperature, S/T_0 does also. The integral of the product of $I(\bar{T}) d\bar{T}$ and S/T_0 is proportional to $h(\tau, \beta)$ and is plotted in Fig. 4 (dotted curve) as a function of reduced delay time τ/T_0.

Both I and h in Fig. 4 are normalized to the same arbitrary peak value to show the effect of the velocity selector on the breadth and shape of the curves. On the reduced transit-time scale h, but not I, is slightly temperature dependent.
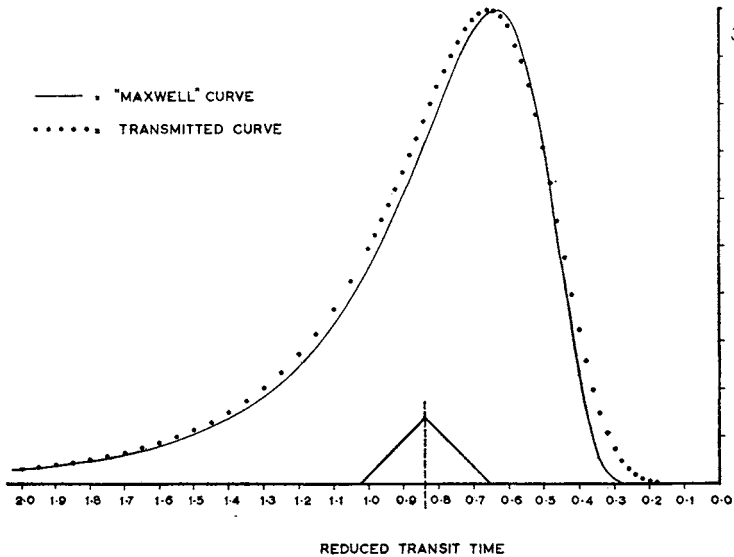

Fig. 4. Maxwell incident beam intensity curve vs. reduced transit-time and theoretical transmitted curve vs. reduced delay time showing effect of transmission through velocity selector. Triangle is ideal shutter function for reduced delay time $= 0.84$.

Appropriate dimensionless forms for I and h which make them directly comparable are given in Appendix I and plotted in Fig. 9.

In calculating theoretical transmission curves to compare with the measured curves, the following effects were considered which could give rise to differences from the dotted curve shown in Fig. 4.

1. The finite angular spread of the beam may be shown to have a negligible effect on the transmitted curve.*

2. The finite disc thickness causes a small but not negligible distortion of the transmitted curve. At twice the most probable transit-time the curve is reduced by 2% relative to the peak.* (This correction was not explicitly introduced in the calculated curves of Figs. 5 and 6.)
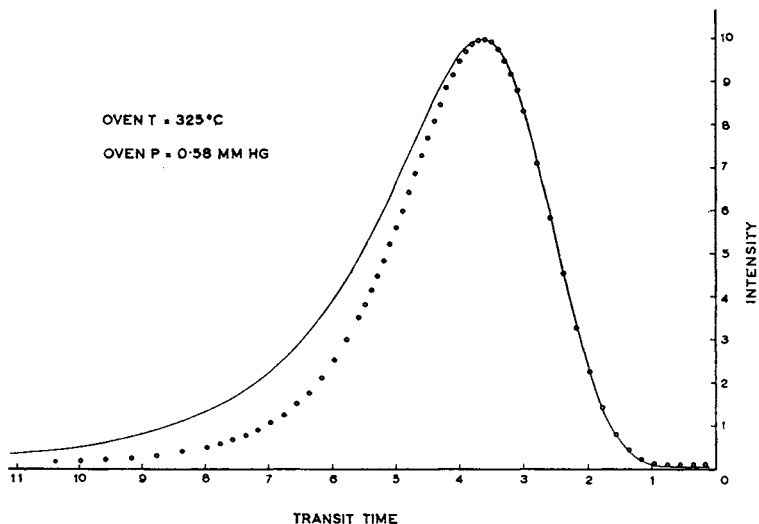
* See Appendix II.

Fig. 5. Measured transmission curve (circles) and calculated Maxwell transmission curve (solid line) at high oven temperature (325° C) and beam intensity. Abscissa is delay time τ, which is approximately transit time of molecules transmitted (1 unit of $\tau = 0.708 \times 10^{-4}$ sec $= 3\frac{1}{3}°$ phase shift). Ordinates are in arbitrary units; curves normalized to same maximum value.
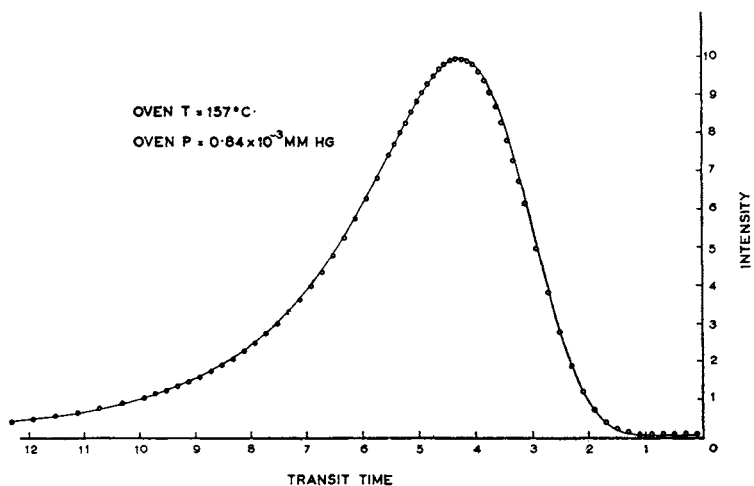

Fig. 6. Measured transmission curve and calculated Maxwell transmission curve at low oven temperature (157° C) and beam intensity. Details as for Fig. 5.

3. The second-order velocity spectrum due to slow molecules with T greater than the time interval between slots gives a small contribution which is a maximum ($\frac{1}{2}\%$ of peak) at zero on the transit-time scale. This correction is taken into account in the calculated curves of Figs. 5 and 6. Third-order and all higher-order spectra taken together have been shown to be negligible.*

IV. Alignment of the Apparatus

The critical measurement for this type of velocity-selector is that of the relative phase angle between the two discs. In order to compare an experimental curve to a calculated curve, one must know not only how much this phase angle changes for a given change in the phase-shifter setting, but also what phase-shifter setting corresponds to zero phase, i.e. to zero transit-time.

That the relative phase angle of the discs is proportional to the setting of the phase-shifter to within 0.1° has been determined by direct visual observation.[3] This was accomplished by inscribing a degree scale on one disc, and a vernier scale on the other. A disc-shaped mirror was placed half-way between the two discs so that the image of the vernier appeared superimposed on the degree scale. The direct observation of phase shift was then made by a stroboscopic flash.

The determination of zero transit-time setting for the molecular beam is accomplished with the aid of a light beam. The photons have effectively zero transit-time compared to molecule transit-times. Thus $I(T)$ for the photons is a delta function at $T = 0$, and the transmitted curve for the light beam is simply the triangular shutter function shown in Fig. 4 (provided the angular spread of the light beam is small). The peak of this triangle indicates zero transit-time, but this will be zero transit-time for the molecular beam only if the light beam and molecular beam are parallel in a "rolled-out" view of the velocity selector—(lack of parallelism shifts the velocity distribution with respect to the light beam peak). The condition of parallelism can be obtained as follows:

(*a*) The difference between the phase-shifter setting corresponding to the peak of the light-beam triangle and the setting corresponding to a definite transit-time on the molecular beam distribution curve is measured (the half-maximum point on the steep side of the curve is usually chosen).

(*b*) The direction of rotation of the discs is reversed, and the measurement described in (*a*) is repeated. (Reversal of rotation of the discs

---

* See Appendix II.

reverses the shift of the velocity distribution with respect to the light beam.)

(c) The molecular beam is adjusted (by moving the detector filament horizontally and in a direction perpendicular to the beam) to make the above two measurements equal. This can be done to within 0.1°, i.e. to within about 1/30 of a unit on the transit time scale of Fig. 5 and 6.

In practice the relative phase angle is never constant in time but fluctuates due to changing torques applied by the motor bearings. In order to keep these fluctuations well below 0.1°, the bearings must be replaced periodically and the motor driving-voltage must be kept sufficiently high. Even with these precautions, a "run-in" time of 15 min. to 1 hour is found to be necessary each time the motors are turned on. During the "run-in" period the relative phase will at first vary quite wildly ($\sim 1°$ or so). The fluctuations then gradually die down to $\sim 0.02°$ if the bearings are in good condition. This much phase shift is easily observable by using either the light beam or the molecular beam.

V. Experimental Results

Figures 5 and 6 are comparisons between experimental results and transmitted curves calculated on the basis of ideal effusion (Maxwell transmission curves). The curves are all normalized to the same maximum value. However, the transit-time scale is fixed by using the measured zero of transit-time and the curves are not adjusted by horizontal translation. The data were taken in a point-by-point fashion in order to eliminate distortion of the distribution curve due to response time of the detector. The zero-line and maximum of the curve were checked frequently during the recording of each distribution in order to minimize the effects of zero-line drift and changes in the beam intensity. In both Fig. 5 and Fig. 6, 18 divisions on the transit-time scale corresponds to a phase shift equal to the angular spacing between the slits in the velocity-selector discs (60° in present case). Therefore, zero on the transit-time scale is also 18 (the second-order spectrum), 36 (the third-order spectrum), etc.

Figure 5 shows an experimental curve for a high oven pressure. The mean free path in the oven is about equal to the slit width. The following features are of interest:

1. The agreement with the calculated curve is very good on the high-velocity side of the maximum, but there is a marked deficiency of low-velocity atoms amounting to about 60% of the calculated value at twice the most probable transit-time.

2. At zero transit-time the experimental curve has roughly twice the amplitude of the calculated curve.

In Fig. 6 the mean free path in the oven is hundreds of times greater than the slit width. Here the important features are:

1. The general agreement on the low-velocity side of the curves is now very good. The deficiency is about 2% of the calculated value at twice the most probable transit-time.

2. The measured intensities at the zero phase position are again in excess of the calculated intensities; the intensities are small (1% of the peak) but measurable. In fact, the experimental curve is higher than the calculated curve from about $9\frac{1}{2}$ onward on the transit-time axis. (After moving the shutter position to reduce its effect on the background signal and decreasing the disc thickness at the slit edge, this excess measured intensity was not observed in later measurements.)

3. Agreement on the high-velocity side is not as good as at the higher oven pressure. There is a 2% deficiency at the half-maximum point.

4. The peak of the measured curve is shifted toward longer transit-times by about 1.5% of the corresponding transit time as compared to the calculated curve.

Effects 3 and 4 can almost be accounted for by the quoted uncertainty in the transit-time measurement. More data are needed to determine if these discrepancies are real.

Figure 7 summarizes the results of ten velocity distribution measurements, each taken at a different oven temperature. All the points refer to a transit time equal to twice the most probable transit time. The scatter on this plot, about 3% (1% of the maximum amplitude), gives some idea of the reproducibility of the data. As noted above there appears to be a residual 2% deficiency present at the lowest oven pressures. Most of this would be removed if the calculated curves had taken into account the thickness of the velocity-selector discs (see Appendix II). However, this also increases the excess which is observed at longer transit-times. (As explained above, this excess was probably spurious. Later measurements made with the shutter positioned at the center of the beam room, rather than directly on the oven side of the collimating slit, have not shown any excess.)

Also plotted on Fig. 7 are two points taken from the potassium data of Miller and Kusch.[2] Bennett's results for knife-edge oven slits indicate low-velocity deficiencies which are several times greater than those reported here. A comparison was also made with the earlier gravity free-fall experiment of Estermann, Simpson, and Stern[5] who used

cesium beams. Their results showed low-velocity deficiencies consider-
ably larger than those reported here for potassium.

The observed deficiency is thus an effect of high beam intensity, and
may arise partly from self scattering in the beam, as roughly calculated
by Estermann, Simpson, and Stern,[5] and partly from deviations from
ideal effusion conditions at the oven slit, when the mean free path is

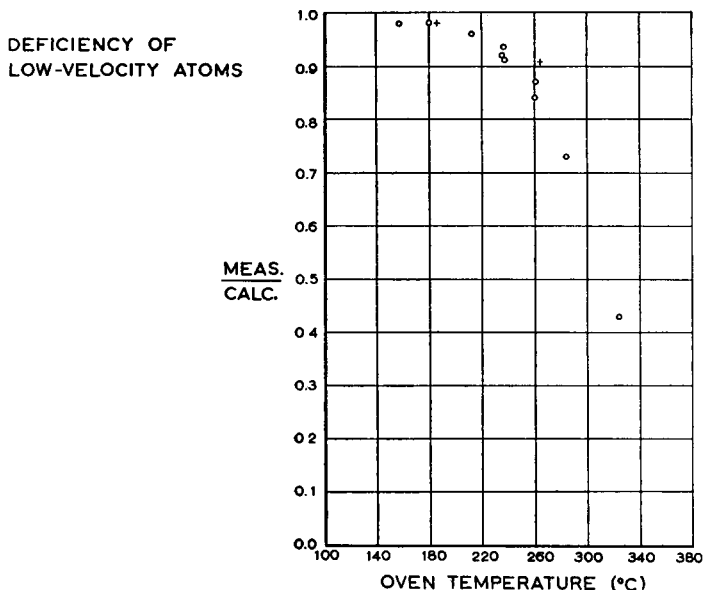Fig. 7. Fraction of transmitted Maxwell intensity observed at twice the most
probable transit-time as a function of oven temperature. $(1 - (\text{meas./calc.}) =$
deficiency.) Circles are the data of this report. Crosses are taken from the data
of Miller and Kusch,[2] Runs No. 57 and 60.

short. The velocity dependence of residual gas scattering at a pressure
5×10^{-7} mm Hg does not appear to be significant, as shown by agree-
ment of measured with calculated transmission curves at the lowest
beam intensities, and by direct calculation assuming quite large scatter-
ing cross-sections (400 Å^2 for K against air molecules). This con-
clusion is in agreement with Miller and Kusch,[2] p. 1320.

The measured and calculated Maxwell transmission curves (corrected
for higher-order spectra) for low-pressure beams agree fairly well in all
respects, although small residual discrepancies as noted above, still per-
sist. The reproducibility and precision should be adequate to detect
the small changes in velocity spectra produced by reflection at solid
surfaces.

REFERENCES

1. A. I. Bennett and I. Estermann, "Distribution of Velocities in Molecular Beams of Potassium", (Doctoral Dissertation, Carnegie Institute of Technology, 1953).
2. R. C. Miller and P. Kusch, Velocity Distributions in Potassium and Thallium Atomic Beams, *Phys. Rev.* **99**, 1314 (1955).
3. A. I. Bennett, The Phase-Shift Velocity Selector (to be published).
4. N. F. Ramsey, "Molecular Beams", Oxford 1956.
5. I. Estermann, O. C. Simpson, and O. Stern, The Free Fall of Atoms and the Measurement of the Velocity Distribution in a Molecular Beam of Cesium Atoms, *Phys. Rev.* **71**, 238 (1947).

APPENDIX I

TRANSMISSION FORMULAS FOR THE PHASE-SHIFT VELOCITY SELECTOR

1. *Definitions and magnitudes of physical quantities*

The following quantities occur in the discussion of the behavior of the velocity selector, and are given here for convenient reference, together with typical magnitudes for the instruments in use.

β = slit open time = 0.850×10^{-4} sec (corresponding to an angular aperture of 4.03°, and rotation speed of the discs of 132 rev/sec).

l = spacing between discs (front surface to front surface) = 19.5 cm.

α = most probable velocity in the oven

$$= \sqrt{\frac{2RT_K}{M}} = 4.611 \times 10^4 \left(\frac{T_K}{500}\right)^{\frac{1}{2}} \frac{cm}{sec}$$

for potassium (T_K = Kelvin temperature).

T = l/v = transit time for molecules of velocity v.

T_0 = l/α = transit time of most probable velocity

$$= 4.229 \times 10^{-4} \left(\frac{500}{T_K}\right)^{\frac{1}{2}} sec.$$

$I(T)dT$ = incident intensity at first disc in range dT (molecules/cm² sec).

$$I_0 = \int_0^\infty I(T)\,dT =$$

= total intensity at first disc (molecules/cm² sec).

τ = time delay of slit in second disc with respect to slit in first disc.

t = time, $t = 0$ when leading edge of slit in first disc first reaches the beam line (the angular spread of the beam is taken as infinitesimal; see Appendix II, 1, for discussions of this approximation).

$h(\tau, \beta)$ = the transmission function, the number of molecules per cm² of beam cross section transmitted during one pass of a pair of slits, for given time delay τ.

Reduced or dimensionless quantities are indicated by a bar.

$\bar{T} = T/T_0$, $\bar{\tau} = \tau/T_0$, $\bar{\beta} = \beta/T_0$ are the reduced transit time, reduced delay time, and reduced slit open time (dimensionless).

Reduced transmission functions $\bar{h}$, and beam intensity functions $\bar{I}$ will be defined later.

2. Derivation and properties of the transmission function

The measured intensity is $h(\tau, \beta)$, (times the frequency at which a slit passes the beam line, 800/sec), which must therefore be related to the intensity distribution in the incident beam $I(T)$. A simple description of this relationship follows from consideration of the pairs of values of T and t', the arrival time at the first disc, which give a transmitted molecule. Figure 8 shows the quadrangular area on a T, t' plane which gives transmission. The first slit is open from $t = 0$ to β,* hence all molecules with arrival times $0 \leqslant t' \leqslant \beta$ pass through it. For each t', there is a range of T for which the molecules reach the second slit during its open time τ to $\tau + \beta$, namely from $T = \tau - t'$ to $T = \tau + \beta - t'$.

$I(T)\,dT\,dt'$ is the number of molecules/cm² arriving at the first disc in range dT during time interval dt', hence

$$h(\tau, \beta) = \int_0^\beta dt' \int_{\tau-t'}^{\tau+\beta-t'} dT\,T\,I(T) = \int_{\tau-\beta}^{\tau} dT \int_{\tau-T}^{\beta} dt'\,I(T) + \int_{\tau}^{\tau+\beta} dT \int_0^{\tau+\beta-T} dt'\,I(T)\dagger \quad \text{(A.1)}$$

* Note it is again open from 15β to 16β, 30β to 31β, etc.

† The actual transmitted intensity at the detector is reduced from $h(\tau, \beta)$ in (A.1) by the square of the source to first disc distance divided by the square of the source to detector distance.
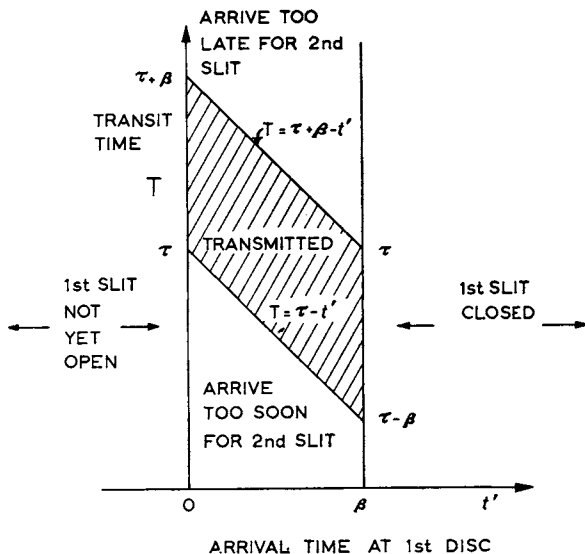
Fig. 8. Transmission diagram of velocity selector. Shaded area shows pairs of transit-times and arrival-times resulting in transmission.

From the second form of (A.1), integrating over t' gives;

$$h(\tau, \beta) = \int_0^\infty S(\tau, \beta, T) I(T) dT \qquad (A.2)$$

where the shutter function $S(\tau, \beta, T)$ is

$$S(\tau, \beta, T) = \begin{cases} T+\beta-\tau & \text{for } \tau-\beta \leqslant T \leqslant \tau \\ \tau+\beta-T & \text{for } \tau \leqslant T \leqslant \tau+\beta. \\ 0 & \text{otherwise} \end{cases} \qquad (A.3)$$

Note that

$$I(T) = 0 \text{ for } T < 0, \qquad (A.4)$$

hence integration in (A.1) and (A.2) for $T < 0$ makes no contribution to $h(\tau, \beta)$.

Differentiating (A.1) twice with respect to τ gives the relationship of h to I, namely

$$\frac{\partial^2 h(\tau, \beta)}{\partial \tau^2} = I(\tau+\beta) - 2I(\tau) + I(\tau-\beta), \qquad (A.5)$$

thus the second derivative of h equals the second finite difference of I at interval β; in compact form,

$$h''(\tau, \beta) = \Delta_\beta^2 I(\tau).$$

One relation satisfied by h is noteworthy: if the pulse of molecules passing the first slit is broken into transit-time ranges by a series of values of τ separated by β, the ranges are contiguous and account for all molecules in the pulse, hence

$$\sum_{n=0,1,2}^{\infty} h(\tau_0 + n\beta, \beta) = \beta \int_0^{\infty} I(T)\, dT = \beta I_0 \; ; \tau_0 < 0. \tag{A.6}$$

The evaluation of $I(T)$ requires solution of the difference equation (A.5) given $h(\tau, \beta)$, hence all derivatives of h, from the measured intensities. Several procedures have been suggested by Bennett.[1,3] We note one useful result. If $\Delta_\beta^2 I(\tau)$ in (A.5) is expanded in derivatives of $I(\tau)$ at τ, only even orders occur, and

$$h''(\tau, \beta) = \beta^2 I''(\tau) + \frac{\beta^4}{12} I^{IV}(\tau) + \dots \tag{A.7}$$

Integration of (A.7) and further differentiation of (A.7) permit its inversion in the form

$$I(\tau) = \frac{h(\tau, \beta)}{\beta^2} - \frac{1}{12} h''(\tau, \beta) + \frac{\beta^2}{240} h^{IV}(\tau, \beta) - \dots \tag{A.8}$$

Evaluation of h and its derivatives from the measurement then permits $I(\tau)$ to be calculated from (A.8).

For calculation purposes it is convenient to define dimensionless beam intensity and transmission functions. Thus $I/I_0 =$ fraction of molecules in the beam per unit transit-time. Hence

$$\bar{I}(\bar{T}) = \frac{T_0 I(T)}{I_0} = \tag{A.9}$$

= the fraction of molecules per unit reduced transit-time, is a dimensionless beam intensity function. It satisfies the condition

$$\int_0^{\infty} \bar{I}(\bar{T})\, d\bar{T} = 1 \; ; \tag{A.10}$$

where $\bar{T} = T/T_0$ is the reduced transit-time variable.

E

Similarly $[h(\tau, \beta)/I_0\beta]$ = fraction of the molecules admitted by the first slit which are in the transmitted pulse for time delay τ and open time β of the slits. Hence

$$\bar{h}(\bar{\tau},\bar{\beta}) = \frac{h(\tau, \beta)}{I_0\beta\,\beta/T_0} = \tag{A.11}$$

= fraction of admitted molecules in transmitted pulse per unit reduced open time, is a dimensionless transmission function comparable to $\bar{I}(\bar{T})$. Thus

$$\sum_{n=0,1,2,\,\cdots}^{\infty} \bar{h}(\bar{\tau}_0 + n\bar{\beta}, \bar{\beta})\left(\frac{\beta}{T_0}\right) = 1$$

by (A.6). Then approximating the sum by an integral, we have

$$\int_{-\bar{\beta}}^{\infty} \bar{h}(\bar{\tau}, \bar{\beta})\,d\bar{\tau} \cong 1 \tag{A.12}$$

where $\bar{\tau} = \tau/T_0$ is the reduced delay time, and for $\bar{\tau} < -\bar{\beta}$, the lower limit, the integrand vanishes. (A.12) is the analogue of (A.10), and shows that the two dimensionless functions $\bar{I}(\bar{\tau})$ and $\bar{h}(\bar{\tau}, \bar{\beta})$ integrated with respect to $\bar{\tau}$ each have unit area, hence are appropriate for comparison to show the transmission effect of the velocity selector on the incident beam.

For the Maxwell intensity distribution (i.e. the intensity distribution in the beam for ideal effusion from an oven in equilibrium at one temperature)

$$\bar{I}(\bar{T}) = \frac{2}{\bar{T}^5}\,e^{-(1/\bar{T})^2}. \tag{A.13}$$

The corresponding distribution in velocity is

$$I(v)dv = 2I_0\frac{v^3}{\alpha^3}\,e^{-v^2/\alpha^2}\frac{dv}{\alpha}$$

(see Ref. 4, p. 20.) The reduced transmission function for this incident intensity is

$$\bar{h}(\bar{\tau}, \bar{\beta}) = \frac{2}{\bar{\beta}^2}[K(\bar{\tau}+\bar{\beta}) - 2K(\bar{\tau}) + K(\bar{\tau}-\bar{\beta})]$$

$$\bar{\beta} = \beta/T_0, \quad K(x) = \frac{x}{2}e^{-(1/x)^2} + \frac{\sqrt{\pi}}{4}\left(\text{erf}\,\frac{1}{x} - 1\right) \tag{A.14}$$

$$\text{erf}\,t = \frac{2}{\sqrt{\pi}}\int_0^t e^{-t^2}dt.$$

A comparison of these functions is shown in Fig. 9, including the effect of the available range of temperature on $\bar{h}(\bar{\tau}, \bar{\beta})$. The velocity selector reduces the peak by about 6 to 9%, and broadens and shifts the distribution slightly with respect to the incident velocity distribution.
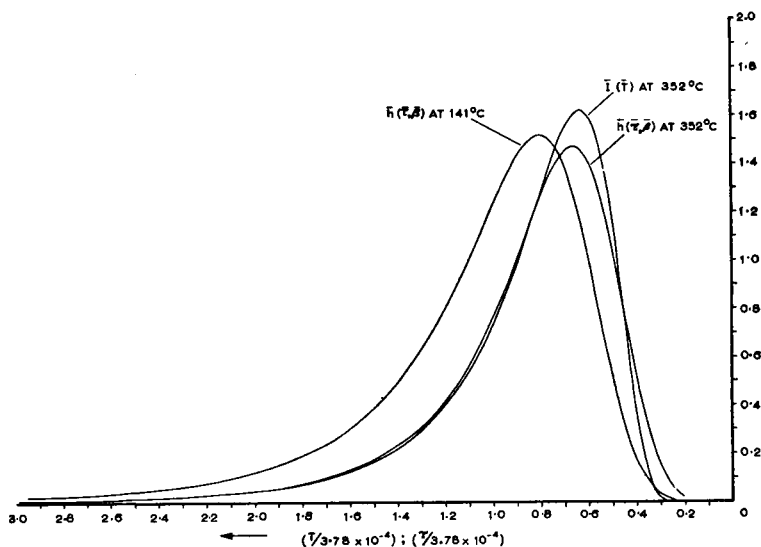

Fig. 9. Reduced Maxwell beam intensity $\bar{I}(\bar{T})$ and reduced transmission functions $\bar{h}(\bar{\tau}, \bar{\beta})$ at extremes of temperature (352° C and 141° C). The scale of τ, or T, is properly reduced at 352° C, where $T_0 = 3.78 \times 10^{-4}$ sec. At 141° C the $\bar{h}$ curve is then *not* plotted against the corresponding $\bar{\tau}$, but shows directly the effect of temperature on the transmission function in terms of the variable τ. (If it were plotted against that $\bar{\tau}$, the $\bar{h}$ for 141° C would lie very close to $\bar{h}$ for 352° C.)

APPENDIX II
CORRECTIONS TO THE IDEAL TRANSMISSION FUNCTION

The function $h(\tau, \beta)$ given by (A.1) is calculated under ideal conditions. Three types of corrections to (A.1) should be considered in

interpreting the measurements made with the actual instrument, and these are now considered quantitatively.

1. *Effects of Finite Angular Spread of the Beam*

The finite angular width (in a plane tangential to the discs) introduces a range of delay times for each value of τ, the time delay of the second disc, since the beam line is now spread out in angle and different parts have different effective delay times. If l is the spacing between discs and φ is the beam angle (in radians), the range of delay times, $2w$, is

$$2w = \frac{l\varphi}{v} = \frac{l}{v}\frac{a}{L} \tag{A.15}$$

where v = velocity of the edge of the disc
   a = detector width
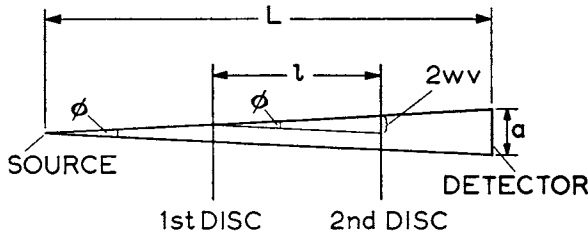 L = oven to detector distance
as shown in Fig. 10.

Fig. 10. Geometry of beam with angular spread φ. Diagram is in a plane which is tangent to the edges of the velocity selector discs.

The effect of this range of delay times is to superimpose a set of transmission functions from $\tau - w$ to $\tau + w$. Using (A.2) for $h(\tau, \beta)$ we can obtain the superposed average transmission function $h_w(\tau, \beta)$ by using an averaged shutter function, $S_w(\tau, \beta, T)$,

$$h_w(\tau, \beta) = \int_0^\infty S_w(\tau, \beta, T)\, I(T)\, dT \tag{A.16}$$

$$S_w(\tau, \beta, T) = \frac{1}{2w} \int_{\tau-w}^{\tau+w} S(\tau, \beta, T)\, d\tau = \frac{1}{2w} \int_{T-w}^{T+w} S(\tau, \beta, T)\, dT \tag{A.17}$$

where

$$S_w(\tau, \beta, T) = \begin{cases} 0 & , T \leqslant \tau - \beta - w \\ \dfrac{(T - \tau + \beta + w)^2}{4w} & , \tau - \beta - w \leqslant T \leqslant \tau - \beta + w \\ T - \tau + \beta & , \tau - \beta + w \leqslant T \leqslant \tau - w \end{cases} \qquad (A.18)$$

$$S_w(\tau, \beta, T) = \begin{cases} \beta - \dfrac{w^2 + (\tau - T)^2}{2w} & , \tau - w \leqslant T \leqslant \tau + w \\ \tau + \beta - T & , \tau + w \leqslant T \leqslant \tau + \beta - w \\ \dfrac{(\tau - T + \beta + w)^2}{4w} & , \tau + \beta - w \leqslant T \leqslant \tau + \beta + w \\ 0 & , \tau + \beta + w \leqslant T \end{cases}$$

Equation (A.18) is the averaged shutter function symmetrical around $T = \tau$, with rounded corners shown in Fig. 11 for an exaggerated value of $\bar{w} = (w/T_0) = 0.025$ and $\bar{\beta} = 0.20$. This function has been used in a direct calculation of $h_w(\tau, \beta)$ from (A.16) for $I(T)$ a Maxwell distribution. The effect is smaller than our precision of measurement and at typical values for our apparatus $(\bar{w} = 0.005, \bar{\beta} = 0.20)$ decreases the ratio of the intensity of slow molecules, say at twice the peak delay time relative to the peak, by about 0.02%. Larger values of w increase this ratio, as is shown in the following table.
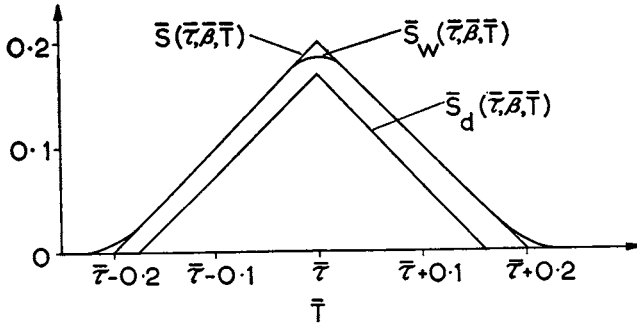

Fig. 11. Reduced shutter functions vs. reduced transit time.
$\bar{S} = (S/T_0)$ ideal shutter function.
$\bar{S}_w = (S_w/T_0)$ shutter function averaged over angular spread of beam.
$\bar{S}_d = (S_d/T_0)$ shutter function corrected for disc thickness.

TABLE 1

EFFECT OF FINITE ANGULAR SPREAD OF BEAM ON TRANSMISSION FUNCTION

(comparing value at $\bar{\tau} = 1.32$ with $\bar{\tau} = 0.66$, corresponding to the peak)

$\bar{w}$	$r_w = \dfrac{\bar{h}_w(1.32, 0.2083)}{\bar{h}_w(0.66, 0.2083)}$	$\%$ change $= \dfrac{(r_w - r_0)100}{r_0}$
0	0.19494	0
0.005	0.19491	−0.02
0.010	0.19506	+0.06
0.020	0.19531	+0.19
0.030	0.19581	+0.45
0.050	0.19740	+1.26
0.100	0.20499	+5.16
0.150	0.21536	+10.5

2. Effects of Finite Disc Thickness

The thickness d of the velocity selector discs decreases the effective open time of both entrance and exit slots for molecules of transit-time T from β to $\beta - (dT/l)$. Thus (l/T) is the velocity of a molecule of transit-time T, hence it must enter one side of the slot at least a time $d/(l/T)$ before the slot closes to clear the other side.

This effective open time evidently alters the ideal shutter function to

$$S_d(\tau, \beta, T) = \begin{cases} \beta - \tau + T\left(1 - \dfrac{d}{l}\right), & \dfrac{\tau - \beta}{1 - \dfrac{d}{l}} \leqslant T \leqslant \tau \\[4mm] \tau + \beta - T\left(1 + \dfrac{d}{l}\right), & \tau \leqslant T \leqslant \dfrac{\tau + \beta}{1 + \dfrac{d}{l}} \end{cases} \qquad \text{(A.19)}$$

The thickness-corrected shutter function $S_d(\tau, \beta, T)$ is still a triangular function of T or τ, with straight sides, but with a lower peak and larger area toward longer transit-times.

Direct numerical integration using $S_d(\tau, \beta, T)$ and the Maxwell beam intensity function shows a reduction in transmission of several per cent at all delay times, least at the peak. The percentage decrease in transmission is shown in Table 2 at the typical value $d/l = 0.005$. The peak value $\bar{h}(\bar{\tau}_p, \bar{\beta})$ is lowered by 3%, where $\bar{\tau}_p$ = the reduced delay time of the peak ($\cong 0.66$), whereas $\bar{h}(2\bar{\tau}_p, \bar{\beta})$ is lowered by 5%, thus creating a relative deficiency at long transit-times that must be considered in interpreting the measured transmission.

TABLE 2

EFFECT OF FINITE DISC THICKNESS ON TRANSMISSION FUNCTION

(at $\bar{\beta} = 0.2083$, and $d/l = 0.005$)

$\bar{\tau}$	$\bar{h}(\bar{\tau}, \bar{\beta})$	$\dfrac{100[\bar{h}(\bar{\tau}, \bar{\beta}) - \bar{h}_d(\bar{\tau}, \bar{\beta})]}{\bar{h}(\bar{\tau}, \bar{\beta})} = \%$ change
0.2	0.0125	6.4
0.4	0.5107	2.9
0.6	1.4339	2.7
0.8	1.2669	3.7
1.0	0.7561	4.8
1.5	0.1742	7.3
2.0	0.0497	9.7
2.5	0.0177	11.9

3. *Effects of Higher-Order Spectra*

The observed transmission function contains all the higher-order velocity spectra resulting from the long transit-time tail of the pulse passing through the first slot. If $\tau_0 = $ the delay time of the next slit after a given one (on the same disc), and $h_t(\tau, \beta)$ the total transmission function to all orders (but uncorrected for angular spread and thickness effects), then

$$h_t(\tau, \beta) = \sum_{n=0}^{\infty} h(\tau + n\tau_0, \beta) \qquad (A.20)$$

where $h(\tau, \beta)$ is the single pass transmission function. In the present design $\bar{\tau}_0$ is about $15\bar{\beta}$, and typical values of the successive spectra, at say, $\bar{\tau} = 0$, and $\bar{\beta} = 0.2083$ of the reduced transmission function $\bar{h}(\bar{\tau}, \bar{\beta})$ are

$$\bar{h}(0, \bar{\beta}) = 0 \, ; \bar{h}(15\bar{\beta}, \bar{\beta}) = 0.007 \, ; \bar{h}(30\bar{\beta}, \bar{\beta}) \simeq 0.0002 \text{ etc.} \qquad (A.21)$$

The sum of all terms after the second term in (A.21) (i.e. after the second-order spectrum) is less than 4% of that term which in turn is about 0.4% of the peak value. Hence the third and higher order spectra can be ignored.